Published in final edited form as:
*Magn Reson Med*. 2014 June ; 71(6): 2051–2058. doi:10.1002/mrm.24871.

# Dynamic metabolic imaging of hyperpolarized [2-$^{13}$C]pyruvate using spiral CSI with alternating spectral band excitation

**Sonal Josan**[1,2], **Ralph Hurd**[3], **Jae Mo Park**[2], **Yi-Fen Yen**[2], **Ron Watkins**[2], **Adolf Pfefferbaum**[1,4], **Daniel Spielman**[2], and **Dirk Mayer**[1,2]

[1]SRI International, Neuroscience Program, 333 Ravenswood Ave., Menlo Park, CA 94025

[2]Stanford University, Department of Radiology, Lucas MRI Center, 1201 Welch Rd. Stanford, CA 94305

[3]GE Healthcare Applied Sciences Laboratory, 333 Ravenswood Ave., Menlo Park, CA 94025

[4]Stanford University, Department of Psychiatry and Behavioral Sciences, 401 Quarry Rd., Stanford, CA 94305

## Abstract

**Purpose—**In contrast to [1-$^{13}$C]pyruvate, hyperpolarized [2-$^{13}$C]pyruvate permits the ability to follow the $^{13}$C label beyond flux through pyruvate dehydrogenase complex and investigate the incorporation of acetyl-CoA into different metabolic pathways. However, chemical shift imaging (CSI) with [2-$^{13}$C]pyruvate is challenging due to the large spectral dispersion of the resonances, which also leads to severe chemical shift displacement artifacts for slice-selective acquisitions.

**Methods—**This work introduces a sequence for 3D CSI of [2-$^{13}$C]pyruvate using spectrally-selective excitation of limited frequency bands containing a subset of metabolites. Dynamic CSI data were acquired alternately from multiple frequency bands in phantoms for sequence testing and in vivo in rat heart.

**Results—**Phantom experiments verified the RF pulse design and demonstrated that the signal behavior of each group of resonances was unaffected by excitation of the other frequency bands. Dynamic 3D $^{13}$C CSI data demonstrated the sequence capability to image pyruvate, lactate, acetylcarnitine, glutamate and acetoacetate, enabling the analysis of organ-specific spectra and metabolite time-courses.

**Conclusion—**The presented method allows CSI of widely separated resonances without chemical shift displacement artifact, acquiring multiple frequency bands alternately to obtain dynamic time-course information. This approach enables robust imaging of downstream metabolic products of acetyl-CoA with hyperpolarized [2-$^{13}$C]pyruvate.

### Keywords

hyperpolarized $^{13}$C; [2-$^{13}$C]pyruvate; dynamic metabolic imaging; spiral CSI

Correspondence: Sonal Josan, SRI International, BN 150, 333 Ravenswood Ave., Menlo Park, CA 94025, sjosan@stanford.edu, Phone: 650-859-3208, Fax: 650-859-2743.

## Introduction

Spectroscopic imaging with hyperpolarized $^{13}C$ compounds enables the measurement of metabolic processes in real time in vivo. The most common substrate, [1-$^{13}C$]pyruvate (Pyr), has been used to monitor the conversion to lactate (Lac), alanine (Ala) and bicarbonate (Bic) as a biomarker for tumor diagnosis, response to therapy and cardiovascular pathologies [1–7]. A number of fast $^{13}C$ spectroscopic imaging techniques have demonstrated the ability to image the metabolism of hyperpolarized [1-$^{13}C$]pyruvate in vivo within the limited lifetime of the hyperpolarized signal. Specialized pulse sequences have been developed focusing on methods including accelerating acquisitions, optimizing signal-to-noise ratio (SNR), quantitation of metabolic kinetics, as well as distinguishing local conversion from inflow [8–18].

Pyruvate is converted to acetyl-coenzyme A (acetyl-CoA) by the enzyme complex pyruvate dehydrogenase (PDC) as a first step toward entering the tricarboxylic acid (TCA) cycle, which is a critical pathway for energy production via oxidative metabolism. Using [1-$^{13}C$]pyruvate, the formation of acetyl-CoA releases the $^{13}C$ label as $^{13}CO_2$/$^{13}C$-bicarbonate which provides a measure of PDC flux, but does not allow an assessment of the fate of acetyl-CoA. Thus, there has also been growing interest in using hyperpolarized pyruvate labeled in the C2 position to track the $^{13}C$ label further downstream into the tricarboxylic acid (TCA) cycle and other metabolic pathways. Some of the metabolic products detected with [2-$^{13}C$]pyruvate in recent studies [19–24] include [1-$^{13}C$]citrate (Cit) in the first span of the TCA cycle, [5-$^{13}C$]glutamate (Glu), which is in exchange with TCA cycle intermediate α-ketoglutarate, [1-$^{13}C$]acetylcarnitine (Alcar) generated from acetyl-CoA via carnitine acetyltransferase (CAT) and [1,3-$^{13}C$]acetoacetate (Aca), which is a ketone body produced from two molecules of acetyl-CoA. These metabolites indicate the incorporation of the $^{13}C$ label from acetyl-CoA into different metabolic pathways.

The majority of the in vivo studies with hyperpolarized [2-$^{13}C$]pyruvate and [1,2-$^{13}C$]pyruvate [20–22] have used a surface coil for localization, obtaining spectra from the entire sensitive volume. Chemical shift imaging (CSI) with [2-$^{13}C$]pyruvate is challenging given the wide spectral dispersion of the resonances, e.g. approximately 160 ppm from [2-$^{13}C$]alanine to [2-$^{13}C$]pyruvate, i.e. ~ 5000 Hz at 3T. Hence, a conventional slice-selective acquisition [23] suffers from severe chemical shift displacement artifact. Additionally, this large frequency range greatly exceeds the practical spectral bandwidth limits of many fast spectroscopic imaging approaches and encoding the entire frequency span can significantly increase the imaging time. The spectral bandwidth to be covered can be reduced by exciting only a single resonance of a smaller sub-band of resonances with a spectrally selective excitation. Cunningham *et al* [8] have demonstrated the use of spectral-spatial excitation for interleaved frequency-specific imaging of individual metabolites with [1-$^{13}C$]pyruvate. Balchandani *et al* [25] presented spectral-spatial excitation and acquisition of different spectral sub-bands in an interleaved manner for $^{1}H$ CSI at 7T. The method presented here uses a spectrally selective excitation to perform 3D CSI of frequency sub-bands with [2-$^{13}C$]pyruvate. Designing a spectral-spatial RF pulse to overcome the slice displacement artifact for the large frequency range of [2-$^{13}C$]pyruvate metabolites while also avoiding any unintended excitation of the metabolites, particularly the injected

substrate, from spectral sidebands is quite difficult and requires long pulse durations. Instead a spectrally selective RF excitation with 3D acquisition was used to mitigate the slice displacement artifact. The spectrally selective pulse design also offers the advantages of being simple to implement with a relatively short pulse duration that makes the sequence less sensitive to T2* decay. The frequency band from 170–185 ppm containing the resonances of [5-$^{13}$C]glutamate (183.8 ppm), [1-$^{13}$C]citrate (180.2 ppm), [1-$^{13}$C]acetylcarnitine (175.2 ppm), [1-$^{13}$C] acetoacetate (177.3 ppm) along with [1-$^{13}$C]pyruvate (172.6 ppm) is of particular interest. A separate excitation is then used to acquire other frequency bands such as [2-$^{13}$C]pyruvate (207.8 ppm) and [2-$^{13}$C]lactate (71 ppm). In this report, dynamic volumetric CSI data were acquired alternately from multiple frequency bands for both phantoms and in vivo rat heart to demonstrate the efficacy of the proposed imaging approach.

## Methods

### RF pulse

A spectrally selective RF pulse with 4-ms duration, passband = ±96 Hz at 1% amplitude loss, FWHM = 674 Hz, maximum $B_1$ of 14 μT for 90° flip angle was used. The RF pulse waveform (a hamming windowed-sinc with time-bandwidth = 2) and its spectral profile are shown in Fig. 1. With the passband centered approximately midway between glutamate and [1-$^{13}$C]pyruvate (this frequency band is referred to as the *Glutamate* band hereon), the passband magnitude at glutamate and $^{13}C_1$-pyruvate resonances (i.e. at ±240 Hz from the center) was 90% of the center, and [2-$^{13}$C]pyruvate signal was not excited (sidelobe null amplitude ~$10^{-5}$ at 968 Hz from passband center). A key requirement of the RF pulse design was adequate suppression of the [2-$^{13}$C]pyruvate peak when exciting the glutamate spectral band, to limit signal contamination from the injected pyruvate aliasing into the acquired frequency band and obscuring the low signal levels of the metabolic products. For the subsequent sampling interval, the RF passband is moved to a different frequency band, e.g. for the [2-$^{13}$C]pyruvate or [2-$^{13}$C]lactate resonances.

### Sample preparation

The samples were polarized via dynamic nuclear polarization using a HyperSense system (Oxford Instruments Molecular Biotools, Oxford, UK). The pyruvate sample used for in vivo experiments consisted of 25 μL of a mixture of 14-M [2-$^{13}$C] pyruvic acid and 15-mM Ox063 (tris(8-carboxy-2,2,6,6-tetrakis(2-hydroxymethyl)benzo(1,2-d-4,5-d′)bis(1,3)dithio-4-yl)methyl) trityl radical (Oxford Instruments, UK) to which 3 μL of a 1:50 dilution of Dotarem (Guerbet, France) was added prior to polarization. The polarized sample was dissolved with a solution of 80 mM NaOH mixed with 40 mM Tris buffer and 0.1 g/L EDTA-$Na_2$, leading to an 80-mM solution of hyperpolarized pyruvate with a pH of 7.4–7.5.

The sample preparation for hyperpolarized phantom experiments utilized co-polarization of [1-$^{13}$C]lactate and [2-$^{13}$C]pyruvate in layers in the same sample cup [26]. For the lactate sample (bottom layer), approximately 70 mg of 1.7-mmol/g [1-$^{13}$C]sodium lactate in a water/glycerol solution with 15-mM OX063 were mixed with approximately 7 μL of a 1:50-solution of Dotarem. After freezing the lactate sample in liquid helium (in the variable

temperature insert of the polarizer), the pyruvate sample (as described above for the in vivo preparation) was added to the cup and the sample was rapidly frozen to avoid mixing the two materials. The same buffer solution was used here as for the pyruvate sample to obtain a solution of 80-mM pyruvate and 40-mM lactate.

### MR experiments

All experiments were performed on a clinical 3T Signa MR scanner (GE Healthcare, Waukesha, WI), using a high-performance insert gradient coil operating at maximum amplitude of 500 mT/m with a slew rate of 1865 mT/m/ms and custom-built transmit/receive $^{13}C$ and $^{1}H$ coils. For phantom experiments, a dual-tuned ($^{1}H/^{13}C$) quadrature transmit-receive RF coil (diameter=50 mm, length=60 mm), operating at 127.9 MHz and 32.2 MHz, respectively, was used. For in vivo experiments, a transmit/receive $^{13}C$ surface coil (inner diameter=28 mm) was placed on the chest over the heart (n=5) or the liver (n=2) with the rat in the supine position. A quadrature volume rat $^{1}H$ coil (diameter=70 mm) was used for anatomical localization and to confirm the position of the $^{13}C$ coil with respect to the organ of interest.

The 3D spiral spectroscopic imaging sequence described in [18] was used with the RF pulse described above. A spiral readout trajectory encoded the spectral and two spatial (x-y) dimensions using 64 echoes and 2 spiral interleaves. The simultaneous encoding of the spectral and spatial dimensions leads to a trade-off between spectral bandwidth and spatial resolution. Achieving a larger spectral width would require a shorter spiral readout, resulting in either a lower spatial resolution or a longer acquisition time with a greater number of interleaves. The slice (z) direction used 12 phase encoding steps in a centric order. Imaging parameters were: FOV=80×80×60 $mm^3$, 5×5×5-$mm^3$ nominal resolution, spectral width=607 Hz, 24 excitations/volume, nominal flip angle of 5° for phantom experiments and 10° for in vivo experiments, TE=3 ms, acquisition time for the volume=2.78 s. The cumulative effect of 24 excitations of 10° each leads to an effective flip angle of 46° for the volume acquisition. The effective flip angle was estimated as $\alpha_{eff} = \cos^{-1}(\cos^{N} \alpha_k)$, where $\alpha_k = 10°$ and N=24, assuming instantaneous successive excitations, ignoring any changes in pyruvate magnetization during the time between excitations. After acquiring a volumetric dataset for one frequency band in 2.8 s, the RF passband was then shifted to another frequency band for the next acquisition. Dynamic data were acquired with the RF passband alternately placed at two different frequency bands for successive time-points. The relevant spectral bands imaged in this study were: (1) *Pyruvate* band for the passband centered on [2-$^{13}C$]pyruvate, (2) *Glutamate* band encompassing the frequency region containing the resonances of glutamate, acetylcarnitine, acetoacetate, [1-$^{13}C$]pyruvate and [1-$^{13}C$]lactate, and (3) *Lactate* band for the passband on the [2-$^{13}C$]lactate doublet.

Accounting for the spiral trajectory sampling and the apodization applied in image reconstruction, the actual in-plane voxel size, as estimated by the integral of the point spread function [27], was 8.0 mm compared to the nominal 5 mm. For the z-phase encode, the effect of apodization and the additional weighting due to the 10° RF sampling (again ignoring any other changes in pyruvate magnetization between excitations) leads to a voxel size of 8.2 mm. It is difficult to quantify the exact voxel size because temporal changes in

the metabolite signal intensity can introduce additional blurring, though that effect is small for the short 2.8 s acquisition duration in this study. Similarly, the effect of T2* decay can also be neglected here given the short 1.3 ms spiral readout length.

### Hyperpolarized phantom

To verify that the alternately excited frequency bands in the 3D CSI sequence did not impact the hyperpolarized magnetization of resonances in the other band over multiple excitations, the $T_1$ relaxation of co-polarized [2-$^{13}$C]pyruvate and [1-$^{13}$C]lactate solution was measured *in vitro.* Of the 3 spectral passbands named above in the RF pulse design section, the pyruvate and the glutamate bands were imaged for the phantom experiments. The [1-$^{13}$C]lactate frequency lies in the passband for the glutamate band. The signal dynamics of the CSI sequence were compared in 3 cases from 3 separate dissolutions: first with the RF passband on lactate and pyruvate in alternate acquisitions every 2.8 s, second where the passband excited lactate only every 5.6 s, and third with pyruvate only excitation every 5.6 s. In all cases, the total scan time was 67.2 s. For each frequency band excited, the resonance of the other substrate was placed in a null at ±968 Hz from the passband center. For the pyruvate excitation, lactate at −968 Hz from the passband center was not excited, while pyruvate was at −234 Hz relative to passband center. Similarly, for the lactate excitation, pyruvate was at +968 Hz and lactate at +234 Hz from passband center. With a nominal 5° flip angle excitation for the passband center, the flip angle at ±234 Hz was 4° given the spectral profile in Fig. 1. Approximately 3 mL of the hyperpolarized solution in a syringe were placed within the RF coil. The time from dissolution to start of 3D CSI was approximately 24 s.

As a reference, the signal dynamics of both resonances acquired with the CSI sequence were also compared to those observed with a free induction decay (FID) pulse-and-acquire sequence over 40 excitations for each of the abovementioned three samples. Immediately after the 3D CSI acquisition ended, a non-selective pulse-and-acquire sequence with an excitation flip angle of 5°, spectral width of 10 kHz and 4096 points was used to acquire $^{13}$C spectra from the same syringe every 3 s over a 2-min period. A 32-μs hard RF pulse was used to achieve a large excitation bandwidth to cover the wide chemical shift of the $^{13}$C resonances. Given the 24 s delay from dissolution to start of the CSI acquisition and its 67 s duration, the time from dissolution to start of FID was approximately 106 s.

### In vivo

Healthy male Wistar rats (n=7, 5 for heart imaging and 2 for liver imaging) were injected with approximately 3 mL of the hyperpolarized pyruvate solution through a tail vein catheter at a rate of approximately 0.25 mL/s. The animals were anesthetized using 1–3% isoflurane, and respiration, rectal temperature, heart rate, and oxygen saturation were monitored throughout the experiment with temperature regulated using a warm water blanket. All animal procedures were approved by the local Institutional Animal Care and Use Committee.

Single-shot fast spin-echo $^{1}$H MR images with nominal in-plane resolution of 0.47 mm and 2-mm slice thickness were acquired in the axial, sagittal, and coronal planes as anatomical

references for prescribing the $^{13}$C CSI experiments. Additional $^{1}$H 3D spoiled gradient echo (SPGR) images (0.625-mm in-plane resolution, 1.25-mm slice thickness, 96 slices) were also acquired matching the $^{13}$C CSI prescription for overlay of the metabolic images.

Dynamic 3D $^{13}$C CSI data were acquired every 2.8 s for 24 time points, starting at the beginning of the pyruvate bolus injection. The time from dissolution to start of injection was approximately 18 s. Of the 24 time-points acquired, the RF passband was placed alternately at the glutamate band and the [2-$^{13}$C]pyruvate band for successive time-points, to acquire 12 time-points for each frequency band. For some scans, the [2-$^{13}$C]pyruvate band was not acquired and the RF passband was alternated between the glutamate band and the [2-$^{13}$C]lactate band instead. For the lactate band, the transmit frequency was placed slightly higher than the down-field peak of the lactate doublet, such that the chemical shift of the [2-$^{13}$C]alanine doublet at about 53 ppm was in the stopband with approximately 1% ripple. This was done to avoid signal contamination from alanine, which would otherwise alias and overlap with lactate given the 607 Hz spectral width of the spiral CSI acquisition.

### Post-Processing

The data were reconstructed similarly as the 3D spiral CSI in [18]. A separate reconstruction was performed for each of the two frequency bands. Metabolic maps were calculated by integrating the signal for each peak in absorption mode using integration widths of ±30 Hz for [2-$^{13}$C]pyruvate and [2-$^{13}$C]lactate (as well as [1-$^{13}$C]lactate in phantom experiments), ±24 Hz for acetylcarnitine, and ±20 Hz for glutamate, acetoacetate and the $^{13}C_1$-pyruvate doublet. The metabolic images from different injections were corrected for differences in the solid-state polarization level of each sample. Metabolite time-courses were calculated from an ROI encompassing the whole syringe in hyperpolarized phantom experiments and an ROI in the heart for in vivo experiments. For the spectra displayed below, a zero-order and first-order phase correction was performed and the baseline was subtracted by fitting a spline to the signal-free regions of the spectrum. The in vivo data shown below were acquired after an infusion of dichloroacetate (DCA) solution (dose of 150 mg/kg dissolved in saline at 30 mg/kg) was administered intravenously over 15 min. DCA was used to stimulate PDH activity [28] and allow acetoacetate detection as little or no acetoacetate signal was detected at baseline in other studies [22,24].

## Results

Figure 2a shows the maps of [2-$^{13}$C]pyruvate and [1-$^{13}$C]lactate overlaid onto $^{1}$H MRI images of the syringe containing the co-polarized solution. A coronal slice reformatted from the 3D axial acquisition is presented. Figure 2b compares the $T_1$ measurements performed with the proposed 3D CSI sequence. The plot shows the magnitude (in logarithmic scale) of the measured [2-$^{13}$C]pyruvate and [1-$^{13}$C]lactate signals, corrected for the effective flip angle, and the linear fits to the data. The data from the individual lactate and pyruvate measurements were normalized to the same signal level as the first CSI measurement acquiring both frequency bands. The $T_1$ values were 37.8 s for lactate and 38.6 s for pyruvate when both resonances were excited alternately. In comparison, the $T_1$ values were 38.4 s for lactate (second sample) and 39.3 s for pyruvate (third sample) when only the

individual resonances were excited. The small difference between the measurements is attributed to normal variation between samples and was also seen in the FID measurements below. The similar $T_1$ values obtained when exciting both frequency bands as compared to a single band demonstrate that the signal behavior of the resonances is not affected by the alternate band excitations.

As a reference, the $T_1$ values obtained from the FID pulse-and-acquire for (lactate, pyruvate) were (32.5 s, 35.9 s) for the first sample, (33.4 s, 36.7 s) for the second sample, and (32.7 s, 36.2 s) for the third sample. The somewhat higher $T_1$ values obtained by the CSI compared to the FID could be due to errors in $B_1$ and calibration of transmit gain (TG) values. Any variation/error in $B_1$ would have a greater effect on the CSI due to the higher effective flip angle for the volume acquisition than the FID pulse-and-acquire sequence. For example, a 10% lower flip angle would change the effective flip angle for the CSI from 19.4° to 17.5° and decrease the $T_1$ by about 3 s, while the corresponding change in FID acquisition would be about 0.3 – 0.4 s in $T_1$ values.

The in vivo time-averaged spectra for the glutamate and lactate frequency bands from a heart ROI are shown in Fig. 3. The spectrum for the glutamate band shows the $^{13}C$ metabolic products of glutamate, acetylcarnitine and acetoacetate from the [2-$^{13}C$]pyruvate bolus injection. The 1% natural abundance [1,2-$^{13}C$]pyruvate doublet ($^{13}C_1$Pyr) in the injected solution was also observed. The dashed line near 170 ppm indicates [2-$^{13}C$]pyruvate signal excited by RF stopband ripples and aliased into the glutamate band. Citrate at 181 ppm was not reliably detected with sufficient SNR and may also overlap with signal from [1-$^{13}C$]pyruvate hydrate. The spectrum for the lactate band shows the [2-$^{13}C$]lactate doublet, which was acquired in alternate time-points with the glutamate band. The RF passband was centered near the down-field peak of the doublet to avoid signal contamination from [2-$^{13}C$]alanine resulting in slightly different flip angles, and hence different signal levels, for the two peaks.

Figure 4 shows representative $^{13}C$ metabolic maps of pyruvate, lactate, acetylcarnitine, glutamate and acetoacetate superimposed onto the corresponding $^{1}H$ image. The central slice of the acquired 3D volume centered on the heart from one rat is shown here. As expected from the high cardiac metabolic activity, the majority of the signal is present at the heart, though it was not possible to differentiate between signal from the ventricular walls and from blood with the resolution used here. A similar spatial distribution was seen in all the rats imaged. The $^{13}C$ images were averaged over all of the 12 time-points acquired for each frequency band to increase the SNR. They were all acquired 10 min after DCA infusion, except for lactate, which was acquired after an additional pyruvate injection 2 h after DCA administration. The [2-$^{13}C$]lactate image is the sum of both peaks in the doublet.

The application of the sequence to the liver is presented in Fig. 5, which shows the time-averaged $^{13}C$ metabolic maps of acetylcarnitine, glutamate and lactate from a slice through the liver for another rat. In contrast to the heart slice, the liver images show a different spatial distribution for the metabolites, with the acetylcarnitine signal arising dominantly from the chest while the glutamate and lactate signals are localized mostly to the liver. The images were averaged from two pyruvate injections, both acquired after DCA infusion. Only

the glutamate band and lactate band were imaged and the pyruvate band was not imaged in this case. The images of acetoacetate are not shown due to insufficient SNR.

The time-courses of the metabolite signals from an ROI in the heart for one animal are plotted in Fig. 6. The SNR of acetaoacetate was not sufficient to plot time-courses. The two panels show the metabolite time-courses after two separate bolus injections of hyperpolarized [2-$^{13}$C]pyruvate – one with acquisition of the glutamate band and the [2-$^{13}$C]pyruvate frequency band (Fig. 6A) and second with acquisition of the glutamate band and the [2-$^{13}$C]lactate band (Fig. 6B). There was no noticeable difference between the time-courses of the metabolic products in the two cases, indicating that removing the excitation on pyruvate to preserve its magnetization for subsequent conversion offered no gain in this case. That is likely due to the high pyruvate inflow in the heart, and may be different for other organs.

## Discussion

The peak at 177.3 ppm is tentatively assigned to acetoacetate. While the heart is not normally a ketogenic organ, McGarry and Foster [29] and Krebs [30] have shown that it can form ketone bodies under certain conditions. As the pyruvate dose in the injected bolus is much higher than physiological level, the excess of acetyl-CoA produced from it after DCA infusion may alter behavior from equilibrium metabolic state leading to production of acetoacetate [29].

With acquisition of 2 frequency bands, the temporal resolution for each spectral band was 5.6 s (2 frequency bands; 2.8 s acquisition per band). Acquisition of all 3 frequency bands (of glutamate, [2-$^{13}$C]lactate and [2-$^{13}$C]pyruvate) interleaved in one scan would increase the sampling interval to more than 8 s. The optimum temporal resolution and the trade-off with number of spectral bands would depend on the specific application.

The signal from the [1,2-$^{13}$C]pyruvate doublet at 1% natural abundance in the glutamate band may be sufficient to provide an estimate of the substrate signal, eliminating the need to image the [2-$^{13}$C]pyruvate band. With the 607 Hz spectral width used here, the aliased signal from [2-$^{13}$C]pyruvate did not overlap with another resonance of interest in the glutamate band. That permits the possibility to allow a small flip angle excitation on [2-$^{13}$C]pyruvate in the RF pulse design and use that signal aliased into the glutamate band to estimate the substrate signal instead of imaging that frequency band separately.

While the current implementation performed CSI on all frequency bands, future sequence modifications could allow acquisition of [2-$^{13}$C]pyruvate, [2-$^{13}$C]lactate and [2-$^{13}$C]alanine using imaging rather than a spectroscopic readout to reduce scan time and allow all metabolites to be acquired in one scan. Another option would be to use a wider passband RF pulse and a different spectral width for the lactate band that would allow acquisition of the alanine doublet in the same band without overlap. However, note that a larger spectral width would require compromising on spatial resolution or longer acquisition time with more spiral interleaves.

With the insert gradients, the spiral CSI sequence achieved 607 Hz spectral width using 2 interleaves and the 3D acquisition took 2.8 s. Using clinical gradients (40 mT/m, 150 mT/m/ms), 8 interleaves would be necessary to achieve the same spectral width and spatial resolution increasing the acquisition time to 11.1 s. While that is still useful for single time-point imaging, the greatly reduced temporal resolution would be unsuitable for tracking metabolite dynamics. However, depending on the application, it may be feasible to reduce the resolution or spectral width in order to reduce the acquisition duration.

Given the high inflow in heart and limited excitation profile of the surface coil, a 10° flip angle with 24 excitations/volume was used for dynamic imaging, though using a different flip angle may provide higher SNR. The sequence also allows using different flip angles for the different frequency bands, e.g. a smaller flip angle for pyruvate than for the metabolic products. As a non-selective RF excitation was employed to avoid chemical shift displacement artifact, the sensitivity profile of the RF coil determines the field of view (FOV) and the number of slice-encoding steps required. The minimum number of slice-encoding steps should be adequate to cover the sensitive region of the receive coil. Instead of a surface coil excitation, the setup can be improved by using a volume coil for homogeneous excitation with a surface coil for reception only.

## Conclusion

This work presents a sequence for fast 3D spiral CSI of hyperpolarized [2-$^{13}$C]pyruvate and its metabolic products using a frequency band-selective excitation and demonstrates results from an in vivo application to rat heart. The sequence overcomes the challenge of the large spectral dispersion of the resonances and allows imaging without chemical shift displacement artifact. Different frequency bands are acquired in an alternating fashion to obtain dynamic time-course information. This approach enables imaging of the metabolic products downstream of acetyl-CoA, thus following the $^{13}$C label incorporation into different metabolic pathways after a [2-$^{13}$C]pyruvate injection.

## Acknowledgments

Funded by: NIH grants AA018681, AA05965, AA013521-INIA, EB009070, P41 EB015891 and GE Healthcare

## References

1. Kurhanewicz J, Vigneron DB, Brindle K, Chekmenev EY, Comment A, Cunningham CH, Deberardinis RJ, Green GG, Leach MO, Rajan SS, Rizi RR, Ross BD, Warren WS, Malloy CR. Analysis of cancer metabolism by imaging hyperpolarized nuclei: prospects for translation to clinical research. Neoplasia. 2011; 13(2):81–97. [PubMed: 21403835]
2. Malloy CR, Merritt ME, Dean Sherry A. Could 13C MRI assist clinical decision-making for patients with heart disease? NMR Biomed. 2012; 24(8):973–979. [PubMed: 21608058]
3. Brindle KM, Bohndiek SE, Gallagher FA, Kettunen MI. Tumor imaging using hyperpolarized 13C magnetic resonance spectroscopy. Magn Reson Med. 2011; 66(2):505–519. [PubMed: 21661043]
4. Golman K, Zandt RI, Lerche M, Pehrson R, Ardenkjaer-Larsen JH. Metabolic imaging by hyperpolarized 13C magnetic resonance imaging for in vivo tumor diagnosis. Cancer Res. 2006; 66(22):10855–10860. [PubMed: 17108122]

5. Kohler SJ, Yen Y, Wolber J, Chen AP, Albers MJ, Bok R, Zhang V, Tropp J, Nelson S, Vigneron DB, Kurhanewicz J, Hurd RE. In vivo 13carbon metabolic imaging at 3T with hyperpolarized 13C-1-pyruvate. Magn Reson Med. 58(1):65–69. 207. [PubMed: 17659629]
6. Day SE, Kettunen MI, Gallagher FA, Hu DE, Lerche M, Wolber J, Golman K, Ardenkjaer-Larsen JH, Brindle KM. Detecting tumor response to treatment using hyperpolarized 13C magnetic resonance imaging and spectroscopy. Nat Med. 2007; 13(11):1382–1387. [PubMed: 17965722]
7. Park I, Larson Peder, Zierhut ML, Vigneron DB, Nelson SJ. Hyperpolarized 13C magnetic resonance metabolic imaging: application to brain tumors. Neuro-oncology. 2010; 12:133–144. [PubMed: 20150380]
8. Cunningham CH, Chen AP, Lustig M, Hargreaves B, Lupo J, Xu D, Kurhanewicz J, Hurd RE, Pauly JM, Nelson SJ, Vigneron DB. Pulse sequence for dynamic volumetric imaging of hyperpolarized metabolic products. J Magn Reson. 2008; 193:139–146. [PubMed: 18424203]
9. Larson PEZ, Hu S, Lustig M, Kerr AB, Nelson SJ, Kurhanewicz J, Pauly JM, Vigneron DB. Fast dynamic 3D MR spectroscopic imaging with compressed sensing and multiband excitation pulses for hyperpolarized 13C studies. Magn Reson Med. 2011; 65(3):610–619. [PubMed: 20939089]
10. Lau AZ, Chen AP, Ghugre NR, Ramanan V, Lam WW, Connelly KA, Wright GA, Cunningham CH. Rapid multislice imaging of hyperpolarized 13C pyruvate and bicarbonate in the heart. Magn Reson Med. 2010; 64(5):1323–1331. [PubMed: 20574989]
11. Mayer D, Yen YF, Levin YS, Tropp J, Pfefferbaum A, Hurd RE, Spielman DM. In vivo application of sub-second spiral chemical shift imaging (CSI) to hyperpolarized 13C metabolic imaging: Comparison with phase-encoded CSI. J Magn Reson. 2010; 204(2):340–345. [PubMed: 20346717]
12. Mayer D, Yen Y-F, Tropp J, Pfefferbaum A, Hurd RE, Spielman DM. Application of subsecond spiral chemical shift imaging to real-time multislice imaging of rat in vivo after injection of hyperpolarized $^{13}C_1$ pyruvate. Magn Reson Med. 2009; 62:557–564. [PubMed: 19585607]
13. Cunningham CH, Chen AP, Albers MJ, Kurhanewicz J, Hurd RE, Yen Y, Pauly JM, Nelson SJ, Vigneron DB. Double spin-echo sequence for rapid spectroscopic imaging of hyperpolarized $^{13}C$. J Magn Reson. 2007; 187:357–362. [PubMed: 17562376]
14. Leupold J, Mansson S, Petersson JS, Hennig J, Weiben O. Fast multiecho balanced SSFP metabolite mapping of 1H and hyperpolarized 13C compounds. MAGMA. 2009; 22(4):251–256. [PubMed: 19367422]
15. Perman WH, Bhattacharya P, Lin AP, Harris KC, Norton VA, Hövener JB, Ross BD. Fast volumetric spatial-spectral MR imaging of hyperpolarized 13C-labeled compounds using multiple echo 3D bSSFP. Magn Reson Imaging. 2010; 28(4):459–465. [PubMed: 20171034]
16. Chen AP, Hurd RE, Cunningham CH. Spin tagging for hyperpolarized 13C metabolic studies. J Magn Reson. 2012; 214:319–323. [PubMed: 22050921]
17. Larson PEZ, Kerr A, Leon Swisher CL, Pauly JM, Vigneron DB. A rapid method for direct detection of metabolic conversion and magnetization exchange with application to hyperpolarized substrates. J Magn Reson. 2012; 225:71–80.10.1016/j.jmr.2012.09.014 [PubMed: 23143011]
18. Josan S, Spielman D, Yen YF, Hurd RE, Pfefferbaum A, Mayer D. Fast volumetric imaging of ethanol metaboism in the rat liver with hyperpolarized [1-$^{13}C$] pyruvate. NMR Biomed. 2012; 25:993–999. [PubMed: 22331837]
19. Schroeder MA, Atherton HJ, Ball DR, Cole MA, Heather LC, Griffin JL, Clarke K, Radda GK, Tyler DJ. Real-time assessment of Krebs cycle metabolism using hyperpolarized 13C magnetic resonance spectroscopy. FASEB J. 2009; 23(8):2529–2538. [PubMed: 19329759]
20. Chen AP, Hurd RE, Schroeder MA, Lau AZ, Gu Y-P, Lam WW, Barry J, Tropp J, Cunningham CH. Simultaneous investigation of cardiac pyruvate dehydrogenase flux, Krebs cycle metabolism and pH, using hyperpolarized [1,2-13C2]pyruvate in vivo. NMR in Biomedicine. 2012; 25:305–311. [PubMed: 21774012]
21. Schroeder MA, Atherton HJ, Dodd MS, Lee P, Cochlin LE, Radda GK, Clarke K, Tyler DJ. The Cycling of Acetyl-Coenzyme A Through Acetylcarnitine Buffers Cardiac Substrate Supply. Circulation: Cardiovascular Imaging. 201210.1161/circimaging.111

22. Josan S, Park JM, Yen Y-F, Hurd R, Pfefferbaum A, Spielman D, Mayer D. In vivo investigation of dicholoroacetate-modulated cardiac metabolism in the rat using hyperpolarized 13C MRS. Proc of ISMRM. 2012:4322.

23. Park JM, Josan S, Yen Y-F, Hurd RE, Spielman DM, Mayer D. Assessment of Dichloroacetate Effect on TCA Cycle Metabolism in Rat Brain In Vivo using MRSI of Hyperpolarized [2-13C]Pyruvate. Proc of ISMRM. 2012:4323.

24. Hu S, Yoshihara HAI, Bok R, Zhou J, Zhu M, Kurhanewicz J, Vigneron DB. Use of hyperpolarized [1-13C]pyruvate and [2-13C]pyruvate to probe the effects of the anticancer agent dichloroacetate on mitochondrial metabolism in vivo in the normal rat. Magn Reson Imaging. 201210.1016/j.mri.2012.05.012

25. Balchandani P, Pauly J, Spielman D. Interleaved narrow-band PRESS sequence with adiabatic spatial-spectral refocusing pulses for 1H MRSI at 7T. Magn Reson Med. 2008; 59:973–979. [PubMed: 18429014]

26. Wilson DM, Keshari KR, Larson PEZ, Chen AP, Hu S, Van Criekinge M, Bok R, Nelson SJ, Macdonald JM, Vigneron DB, Kurhanewicz J. Multi-compound polarization by DNP allows simultaneous assessment of multiple enzymatic activities in vivo. J Magn Reson. 2010; 205(1): 141–147. [PubMed: 20478721]

27. Golay X, Gillen J, van Zijl PCM, Barker PB. Scan time reduction in proton magnetic resonance spectroscopic imaging of the human brain. Magn Reson Med. 2002; 47:384–387. [PubMed: 11810683]

28. Stacpoole PW. The pharmacology of dichloroacetate. Metabolism. 1989; 38(11):1124–1144. [PubMed: 2554095]

29. McGarry JD, Foster DW. Ketogenesis and Cholesterol Synthesis in Normal and Neoplastic Tissues of the Rat. J Biol Chem. 1969; 244:4251–4256. [PubMed: 4308173]

30. Krebs HA. Rate control of the tricarboxylic acid cycle. Advances in Enzyme Regulation. 1970; 8:335–353. [PubMed: 4920378]

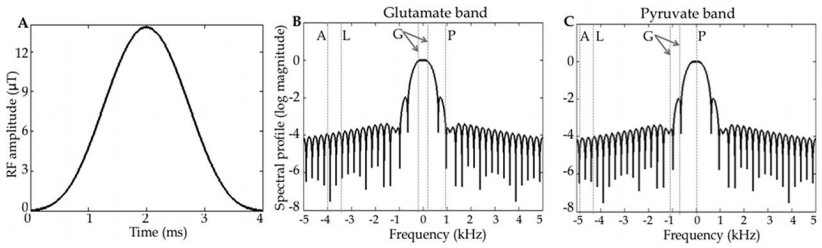


**Figure 1.**

The spectrally selective hamming windowed-sinc RF pulse (Fig. A) and its spectral profile in log scale with passband placed on the glutamate band (Fig. B) and on the pyruvate band (Fig. C). The dashed lines marked G indicate the chemical shifts of [5-$^{13}$C]glutamate and [1-$^{13}$C]pyruvate in the passband with the resonances of acetylcarnitine, acetoacetate and citrate located between them. With the passband placed on the glutamate band, signal from [2-$^{13}$C]pyruvate (line P) is suppressed. Lines L and A mark the locations of [2-$^{13}$C]lactate and [2-$^{13}$C]alanine, respectively. To image [2-$^{13}$C]pyruvate or [2-$^{13}$C]lactate, the passband is shifted to the corresponding frequency.

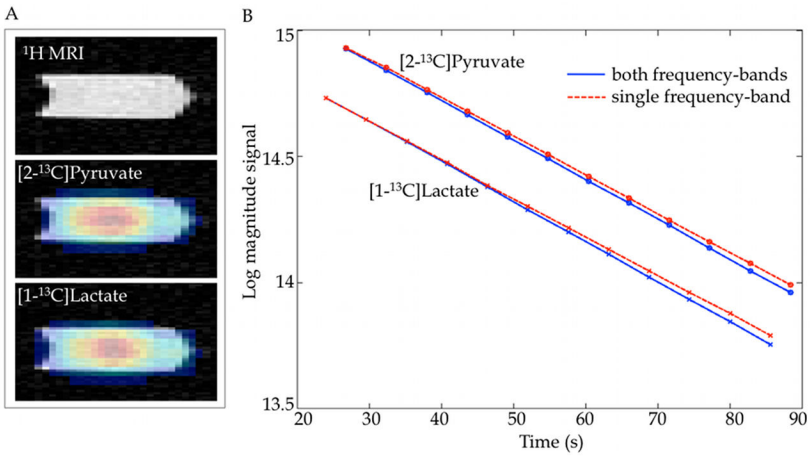


**Figure 2.**

(A) $^{1}$H SPGR MRI and overlaid $^{13}$C metabolic images of a coronal slice (reformatted from 3D axial acquisition) through the syringe containing co-polarized [2-$^{13}$C]pyruvate and [1-$^{13}$C]lactate solution. (B) Comparison of in vitro $T_1$ measurements for a co-polarized solution of [2-$^{13}$C]pyruvate and [1-$^{13}$C]lactate when both resonances were imaged in an interleaved manner (solid blue line) with the excitation/acquisition of each band individually (dashed red line) using 3D CSI with frequency band-selective excitation. The similar $T_1$ values obtained demonstrate that the excitation of one band did not affect the signal behavior of resonances in the other band.

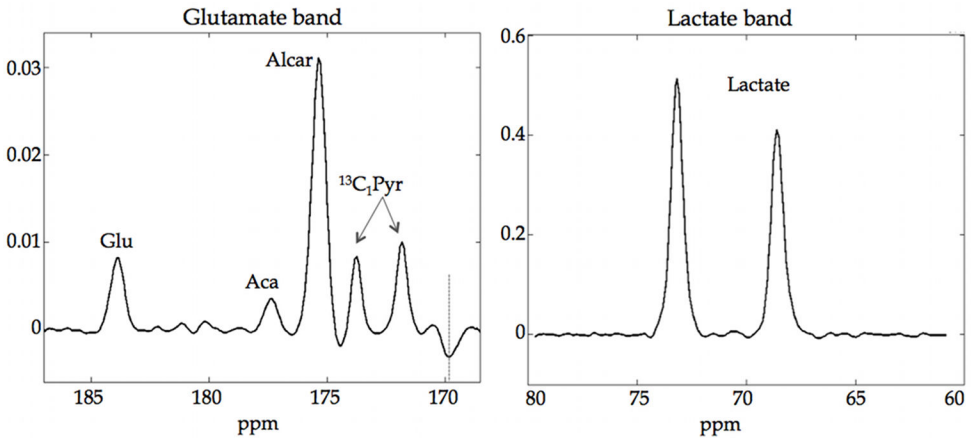


**Figure 3.**

(left) Spectrum of the glutamate frequency band averaged over all time-points acquired from rat heart in vivo showing the $^{13}C$ resonances of glutamate (Glu), acetoacetate (Aca), acetylcarnitine (Alcar) as well as natural abundance [1,2-$^{13}C$]pyruvate doublet ($^{13}C_1$Pyr) in the injected solution. The dashed line near 170 ppm indicates [2-$^{13}C$]pyruvate signal excited by RF stopband ripples and aliased into the glutamate band. Citrate at 181 ppm was not reliably detected with sufficient SNR and may overlap with signal from [1-$^{13}C$]pyruvate hydrate. (right) Time-averaged spectrum of the lactate band acquisition showing the [2-$^{13}C$]lactate doublet acquired from the same rat. The RF passband was centered near the down-field peak of the doublet to avoid signal contamination from [2-$^{13}C$]alanine resulting in slightly different flip angles for the two peaks.

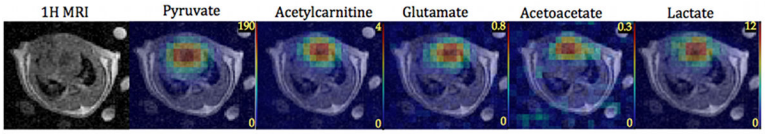


**Figure 4.**

Time-averaged $^{13}C$ metabolite maps from a bolus injection of hyperpolarized [2-$^{13}C$]pyruvate superimposed on to $^{1}H$ MR images for one rat. The central slice of a 3D acquisition centered on the heart is shown. The images were acquired at 10 min after dichloroacetate infusion, except for [2-$^{13}C$]lactate, which was acquired 2 h post-DCA from a separate [2-$^{13}C$]pyruvate injection.

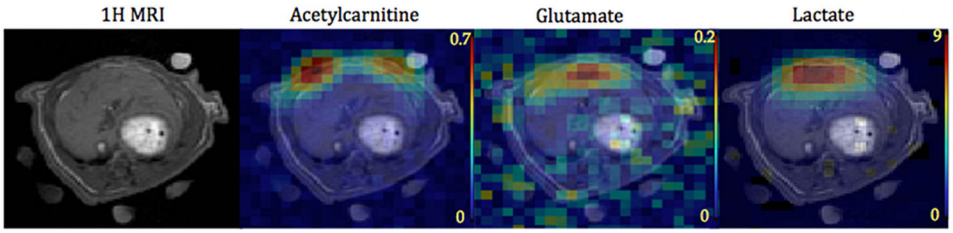


**Figure 5.**

Time-averaged $^{13}C$ metabolite maps of a slice through the liver superimposed on to $^{1}H$ MR images. A central slice from a 3D acquisition centered on the liver is shown. The images were averaged from two injections of hyperpolarized [2-$^{13}C$]pyruvate. Only the glutamate band and lactate band were imaged and the pyruvate band was not imaged in this case. The acetylcarnitine resonance lies within the glutamate frequency band.

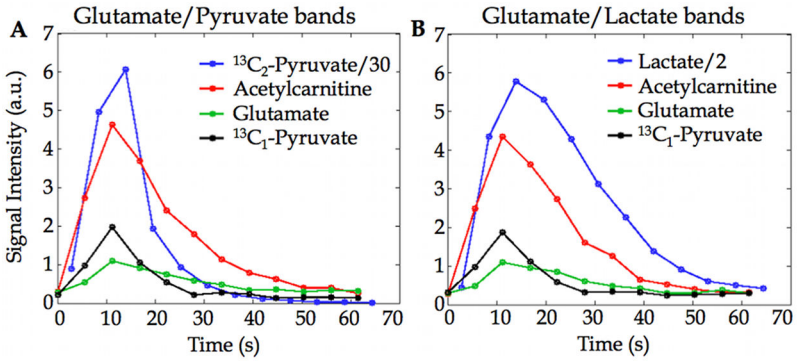


**Figure 6.**

Metabolite signal time-courses from heart ROI after bolus injections of hyperpolarized [2-$^{13}$C]pyruvate with alternate acquisition of (A) the glutamate frequency band and the [2-$^{13}$C]pyruvate band or (B) the glutamate band and the [2-$^{13}$C]lactate band. The glutamate, acetylcarnitine and [1-$^{13}$C]pyruvate signals are from the glutamate band acquisition. The SNR of acetoacetate was insufficient to plot time-courses. The $^{13}C_1$-pyruvate signal is from the $^{13}C_1$-$^{13}C_2$ doublet from natural abundance [1,2-$^{13}$C]pyruvate in the injected [2-$^{13}$C]pyruvate solution.